Donor–Acceptor Systems

Deutsche Ausgabe: DOI: 10.1002/ange.201501414
Internationale Ausgabe: DOI: 10.1002/anie.201501414

Revealing the Charge-Transfer Interactions in Self-Assembled Organic Cocrystals: Two-Dimensional Photonic Applications**

*Weigang Zhu, Renhui Zheng, Xiaolong Fu, Hongbing Fu, Qiang Shi, Yonggang Zhen, Huanli Dong, and Wenping Hu**

Abstract: *A new crystal of a charge-transfer (CT) complex was prepared through supramolecular assembly and it has unique two-dimensional (2D) morphology. The CT nature of the ground and excited states of this new Bpe-TCNB cocrystal (BTC) were confirmed by electron spin resonance measurements, spectroscopic studies, and theoretical calculations, thus providing a comprehensive understanding of the CT interactions in organic donor–acceptor systems. And the lowest CT_1 excitons are responsible for the efficient photoluminescence ($\Phi_{PL} = 19\,\%$), which can actively propagate in individual 2D BTCs without anisotropy, thus implying that the optical waveguide property of the crystal is not related to the molecular stacking structure. This unique 2D CT cocrystal exhibits potential for use in functional photonic devices in the next-generation optoelectronic communications.*

Organic multifunctional semiconductors are emerging as high-demand materials because of their appealing and versatile applications in advanced optoelectronics. Since limited success has been achieved through traditional structural tailoring of single-component materials, the supramolecular assembly[1] of two different materials into crystals through noncovalent interactions (crystallization is a typical phenomenon of self-assembly), such as charge-transfer (CT) and π–π interactions, and hydrogen and halogen bonds, provides an optional strategy.[2–6] Organic cocrystals (as defined previously[7–9] and generally accepted[1,2]) with an ordered stacking of donors (D) and acceptors (A) show unique physicochemical properties,[10–13] which are not simply the sum of the properties of the constituent compounds. For example, ambipolar charge-transport behavior[14] and strong white-light-emitting properties[15] have been observed in the cocrystals of CT complexes. These features are exciting, but as Wuest proposed,[16] "effective cocrystallization is not easy to achieve, because introducing additional components can alter overall properties in unpredictable ways". This proposal indicates that not just any two types of materials can recognize each other and aggregate into cocrystals in which intermolecular interactions play a significant role. Generally, cocrystals with irregular shapes are obtained as a result of weak interactions,[17,18] whereas strong CT interactions, as a driving force for self-assembly, are observed in common cocrystals with D–A stacking, thus leading to one-dimensional (1D) supramolecular structures.[2,12] In contrast, organic cocrystals with uniform 2D morphology (2D cocrystals) are little reported, but are desired because of their potential applications in graphene-like optoelectronics, field-effect transistors (FETs),[19] whispering-gallery-mode (WGM) lasers,[20] and optical planar diodes,[21] as well as because of their fundamental interest for anisotropic studies. Therefore, the random assembly of different materials into cocrystals with a desired morphology and function remains a challenge.

For the crystals of D–A complexes, one of the most important issues is confirming the CT interactions, partially because the degree of CT is related to the conducting ability[22,23] and lattice instability[24] of cocrystals. To the best of our knowledge, the CT nature of crystals of D–A complexes is difficult to verify accurately. For instance, the ground state of the crystal of the perylene-TCNQ complex is neutral, whereas the first electronic excited state is a CT band peaking at $\lambda = 960$ nm.[25,26] Thus, in previous reports[27,28] the absorption spectra of a mixed solution may not be a perfect approach to confirm the existence of CT interactions in D–A dyads. The molecular interactions in the solid state are quite different from those in solution and the CT interactions seem to be enhanced after cocrystallization of the DPTTA-DTTCNQ system.[14] In contrast, the CT interactions and exciton dynamics are more crucial to the light-emitting[29,30] and photoconductivity[31–33] properties of organic cocrystals, and is not yet well understood.[34,35] Similarly, Yan and co-workers[18] have demonstrated a cocrystal strategy to tune luminescent properties of solid-state materials and the variations of optical properties are attributed to the formation of an excimer. This formation, however, conflicts with the result of the high photoluminescence quantum yield (PLQY, Φ_{PL}) of 25.6 % and shortened fluorescence lifetime. Anyway, the CT interaction and its effects on optoelectronic features of organic D–A cocrystals are still largely elusive.

[*] W. G. Zhu, Dr. R. H. Zheng, X. L. Fu, Prof. H. B. Fu, Prof. Q. Shi, Dr. Y. G. Zhen, Dr. H. L. Dong, Prof. W. P. Hu
Institute of Chemistry, Chinese Academy of Science (ICCAS)
Beijing 100190 (China)
E-mail: huwp@iccas.ac.cn
W. G. Zhu, X. L. Fu
University of Chinese Academy of Science
Beijing 100049 (China)

[**] We sincerely thank Dr. Libo Du for ESR measurements, Dr. Ye Zou for XPS analysis, Xuedong Wang for PLQY measurements, and Zhenyi Yu for PL lifetime characterizations. This work was supported by the National Natural Science Foundation of China (51303185, 21021091, 51033006, 51222306, 51003107, 61201105, 3591027043, 91222203, 91233205, 21473222), the China-Denmark Co-project, TRR61 (NSFC-DFG Transregio Project), the Ministry of Science and Technology of China (2011CB808400, 2011CB932300, 2013CB933403, 2013CB933500, 2014CB643600), and the Chinese Academy of Sciences (the Strategic Priority Research Program, Grant No. XDB12020300).

Supporting information for this article is available on the WWW under http://dx.doi.org/10.1002/anie.201501414.

 © 2015 Wiley-VCH Verlag GmbH & Co. KGaA, Weinheim

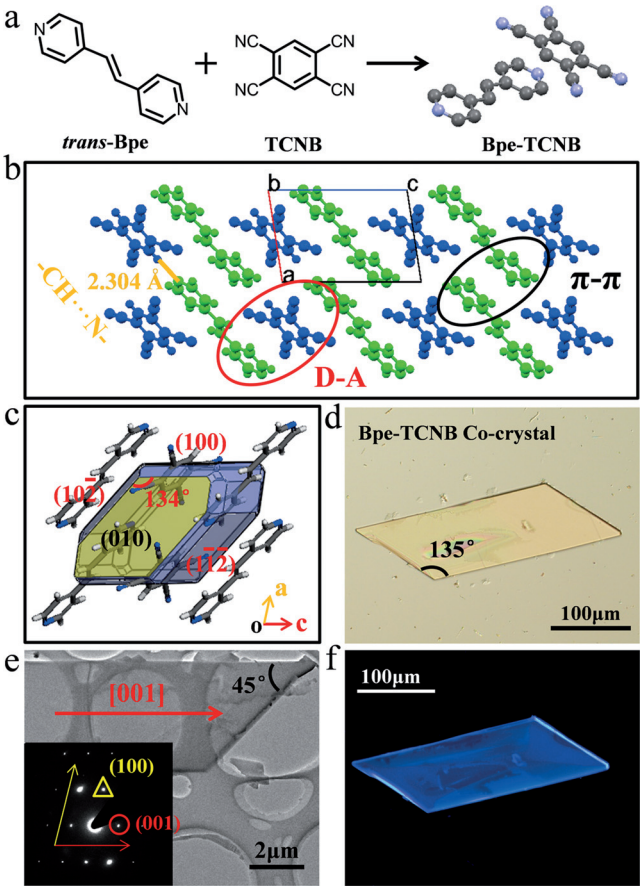

Figure 1. a) Chemical structure of *trans*-Bpe, TCNB, and the molecular structure of the resulting Bpe-TCNB complex. b) The self-assembly driving forces. c) The predicted equilibrium morphology of the cocrystal. d) Optical image of BTC on the glass substrate. e) TEM and SAED images of individual BTCs. f) CLSM image of BTC on a glass substrate.

Herein, a new cocrystal of a D–A complex (1:1) with a uniform 2D parallelogram-like shape was obtained by supramolecular assembly of 1,2-di(4-pyridyl)ethylene (*trans*-Bpe) and 1,2,4,5-tetracyanobenzene (TCNB) molecules (Figure 1a). Further experimental and theoretical evidence confirms that both the ground and excited states of the Bpe-TCNB cocrystals (BTCs) are CT states and the lowest CT_1 excitons are responsible for efficient violet-blue luminescence. Moreover, this 2D cocrystal can serve as an active optical waveguide which allows photons to propagate without anisotropy, thus indicating that the optical waveguide property has nothing to do with molecular packing structure. We demonstrate that this cocrystal can function as a photonic resistor and planar-light propagation modulator in future optoelectronic communications.

The D–A interaction was found in the mixed acetonitrile solution of Bpe and TCNB. The well-structured absorption spectra of the Bpe and TCNB monomers (see Figure S1 in the Supporting Information) are consistent with previous reports.[36,37] Interestingly, when the concentration of TCNB (C_{TCNB}) increases in the solution ($C_{Bpe} = 1.65 \times 10^{-5}$ M), the absorption intensity initially decreases (see Figure S2) and then increases when C_{TCNB} reaches above 1.65×10^{-5} M. The increase of absorption intensity results from the added TCNB component, while the reduction indicates the D–A interaction between Bpe and TCNB.[38] This interaction will play an important role in the followed progress of solution drop-casting (a common self-assembly method).

The BTCs consist of segregated D and A molecular columns (see Figure S3a) with an intermolecular D–D distance of 3.38 Å and D–A distance of 3.30 Å (see Figure S3c), both of which are shorter than the sum of the van der Waals radii (3.4 Å) of carbon atoms, thus giving rise to significant π–π and D–A interactions, respectively (see Figure S3d). The two types of strong interactions and intermolecular -N···HC- interactions (see Figure S3e), as self-assembly driving forces along distinct directions, make molecules aggregate and expand into a layered structure (see Figure S3f), thus leading to a unique crystal shape rather than common 1D wires or rods.[2,15] These noncovalent interactions are clearly shown in Figure 1b. And the equilibrium morphology of BTCs, as predicted by materials studio software, reveals a blocklike crystal with its dominant (010) plane possessing an intersection angle of 134° as shown in Figure 1c. Hence, in this 2D assembly the -N···HC- interaction (2.30 Å) is responsible for (100) growth, while π–π and D–A interactions contribute to the cocrystal's growth along [001]. Despite these analyses, BTCs were prepared by directly drop-casting an acetonitrile solution of Bpe and TCNB onto a glass substrate. Optical images (Figure 1d) confirm that the 2D parallelogram-shaped BTCs have an intersection angle of 135°, which is significantly different from that of Bpe or TCNB crystals (see Figure S4). Figure 1e displays the transmission electron microscope (TEM) image and the selected area electron diffraction (SAED) pattern recorded from individual BTCs, thus showing single crystalline nature. Triclinic BTCs (see Table S1) belong to the space group of $P\bar{1}$, with cell parameters of $a = 6.88$ Å, $b = 7.11$ Å, $c = 10.23$ Å, $\alpha = 77.49°$, $\beta = 78.61°$, $\gamma = 75.69°$. And the BTC can be indexed as shown in Figure 1e, thus corresponding well with the X-ray diffraction (XRD) results (see Figure S5), in which only (010) and (020) peaks appear. Therefore, the morphology and structural characterizations are the same as the predicted results. Moreover, the Raman spectra (see Figure S6) suggest that the highly crystalline parallelogram-shaped crystal is indeed a composite of Bpe and TCNB materials. The confocal laser scanning microscope (CLSM) image of BTCs (Figure 1f) shows a strong violet-blue photoluminescence (PL) under the excitation of unfocused UV light.

Spectroscopic studies were then conducted to determine the CT nature and photophysical properties of BTCs. Figure 2a displays the absorption spectra of the crystals and a new and largely red-shifted absorption peak appears around $\lambda = 363$ nm (see Figure S7), which is attributed to the CT transitions. The CT nature of the ground state of BTCs was also confirmed by ESR measurements (Figure 2b). A relatively weak but sharp resonance signal is centered at 3473 T, thus indicating the existence of active radicals. The g factor is calculated to be 2.0022 according to the ESR theory, and is almost equivalent to the free-electron value of 2.0023. Hence, the ESR spectrum reveals the existence of unpaired electrons

© 2015 Wiley-VCH Verlag GmbH & Co. KGaA, Weinheim

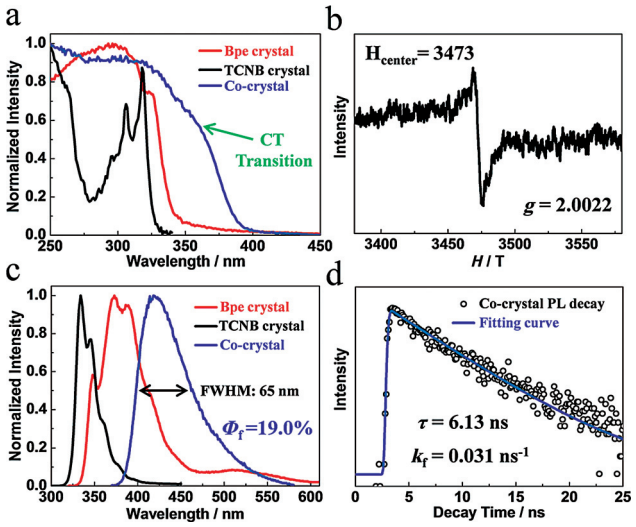

Figure 2. a) The absorption spectra of Bpe, TCNB, and Bpe-TCNB crystals. b) The ESR spectrum of BTCs. c) PL spectra of Bpe, TCNB, and Bpe-TCNB crystals. d) Typical PL decay profile of BTCs on a glass substrate.

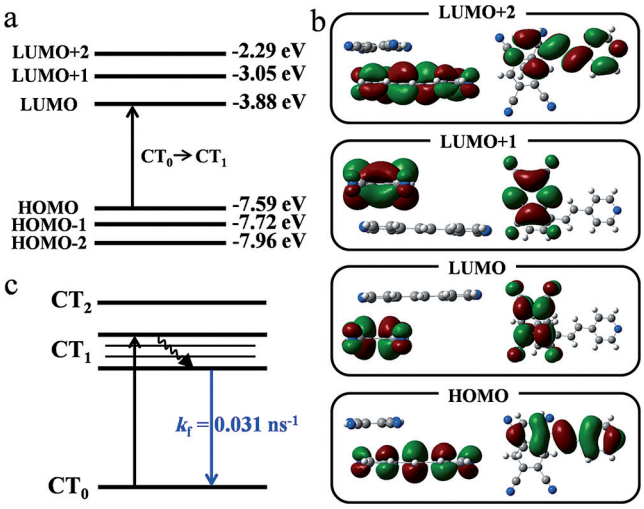

Figure 3. a) The calculated energetic diagram of BTCs. b) MO diagrams for the cocrystals as calculated by TD-DFT. c) The Jablonski diagram for CT transitions of BTCs.

in the BTCs. And the X-ray photoelectron spectroscopy (XPS) profile of the cocrystals (see Figure S8) shows a shifted N1s peak (400.52 eV),[39] as compared with those of the single-component powder, and clearly demonstrated the appearance of Bpe N^+, thus indicating the CT interactions between Bpe and TCNB. These data allow us to conclude that the ground state of the BTCs is a CT state.

The PL spectrum of the BTCs (Figure 2c) is shifted bathochromically with a new structureless and broad peak (FWHM: 65 nm) located at $\lambda = 420$ nm, as compared with those of the single-component crystals. The Stokes shift (see Figure S9) has a value of 3739 cm^{-1} and indicates a large molecular configuration change and strong electronic communication in the excited state, and the fluorescence originates from a dimolecular species rather than a monomeric one. In addition, the PLQY of the BTCs was measured to be 19.0%, while the PL lifetime (τ) is 6.13 ns (Figure 2d). The mono-exponential decay of PL intensity implies that the fluorescence of the BTCs originates from one excited state without competing radiative deactivation process. The radiation rate constant (k_f) is calculated to be 0.031 ns^{-1} by using the equation $K_f = \Phi_{PL}/\tau$, and it is very near to the value of typical crystals of a CT complex,[12,15,34] but smaller than those of single-component crystals.[40,41] These behaviors of the excited state of the BTCs illustrate its CT nature.

Theoretical calculations were performed to gain a deeper understanding of this cocrystal (Figure 3). A total Mulliken charge (see Figure S10a) of 0.0788 on the donor Bpe moiety, and a static dipole moment (SDM) of 0.95 Debye with the vector pointing towards Bpe (see Figure S10b,c) confirms the CT from Bpe to TCNB. This transfer was further verified by the calculated lowest unoccupied molecular orbital (LUMO) and the highest occupied molecular orbital (HOMO) of BTCs (Figure 3b). Here we know that as a result of the molecular interactions in the ground state of this D–A cocrystal, the CT process goes from the HOMO of Bpe to the LUMO of TCNB and the electron cloud rearranges over the D–A units, thus forming new molecular orbitals (MOs). Therefore, the electronic transitions occur between these new MOs from the ground CT state to excited CT states. The absorption spectra of the BTCs were calculated and the electronic transitions were assigned as displayed in Figure 3a, as well as Figure S11 and Table S2. The HOMO→LUMO excitation contributes to the lowest electronic transition ($CT_0 \rightarrow CT_1$) with an oscillator strength (f) of 0.0077 and the energy of this CT transition (3.0 eV, 413 nm) is close to that of the experimental result (3.42 eV, 363 nm).[2] The corresponding transition dipole moment (TDM) of 0.82 Debye points from Bpe toward TCNB (see Figure S11c). And the observed band peaked at $\lambda = 328$ nm (3.78 eV) is attributed to the $CT_0 \rightarrow CT_2$ transition, which arises from HOMO→LUMO + 1 excitation (calculated at 3.80 eV, 326 nm). The main CT band ($CT_0 \rightarrow CT_3$) is calculated at $\lambda = 274$ nm (4.52 eV), primarily for the HOMO→LUMO + 2 excitation (73.9%), and accords well with experiments. Besides these absorptions, the fluorescent state is considered to be the lowest CT state (CT_1 state), since a good mirror image relation between absorption and fluorescence spectra is observed (see Figure S9b).

The experimental and theoretical evidence help draw a picture of CT excitons evolution following primary photoexcitation to their recombination to the ground state. This photophysical progress of the BTCs can be illustrated as displayed in Figure 3c. When excited, photons are absorbed to give optical transitions from the ground CT_0 state to excited CT_n states, and then relax to the lowest CT_1 state to fluoresce. The CT_1 excitons are generated, delocalize, and recombine in the BTCs, and are responsible for PL, thus arousing our interests in related optoelectronic properties.

The excited PL can actively propagate in two distinct directions within these 2D BTCs and out-couple at the edge tips. In a typical experiment, spatially resolved PL imaging and spectroscopy characterizations were conducted on a homemade platform with the excitation of a $\lambda = 374$ nm

 © 2015 Wiley-VCH Verlag GmbH & Co. KGaA, Weinheim

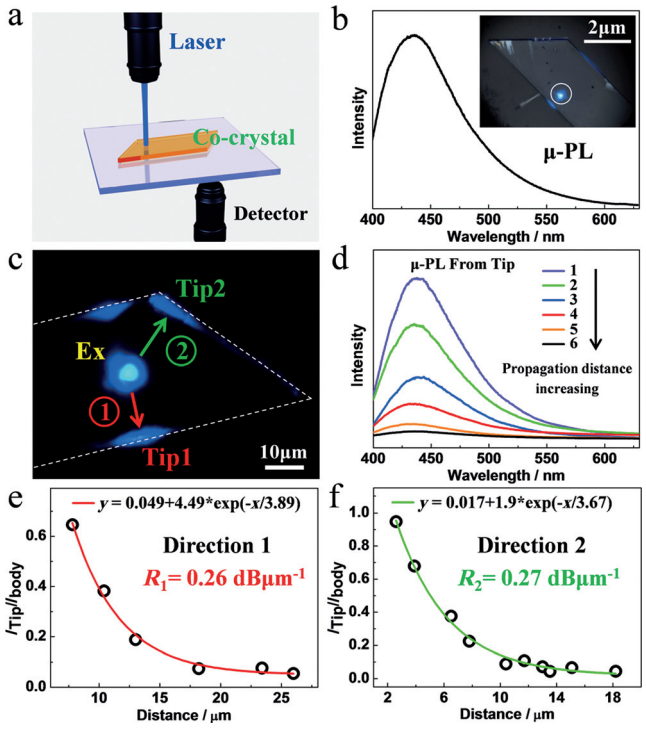

Figure 4. a) Schematic diagram of the platform for optical waveguide. b) μ-PL of BTC (inset shows the optical image of BTC under excitation). c) PL microscopy image of BTC under excitation. d) μ-PL collected from the tip as the propagation distance increases. The dependence of the intensity ratio I_{tip}/I_{body} on the propagation distance along direction 1 (e) and direction 2 (f).

laser beam (Figure 4a). The micro-area photoluminescence spectra (μ-PL) of BTCs were collected (Figure 4b) and show only a peak located at $\lambda = 436$ nm, thus indicating a red-shift of 16 nm as compared with steady PL spectra. As depicted in Figure 4c, when the laser is focused on BTC, photons are confined and propagate parallel to the substrate in two different directions with an intersection angle of 45° (see Figure S12). The 2D crystal is of great importance for an anisotropy study and we focused on the characterization of the loss of optical propagation. Typically, the μ-PL intensity of the tip greatly decreases when moves the laser excitation spot to increase the PL propagation distance (Figure 4d). The PL intensity at the excited site (I_{body}) and at the light-emitting tip (I_{Tip}) were recorded and the dependence of the intensity ratio, I_{Tip}/I_{body}, on the distance in two directions are shown in Figures 4e and 4f, respectively. The data points clearly show a nearly exponentially decay and they can be fitted by a single exponential decay function $I_{Tip}/I_{body} = A\exp(-RD)$, where D is the propagation distance between the excited spot and the emitting tip and A is a constant. Therefore, the optical propagation loss coefficient (R) along direction 1 (R_1) and direction 2 (R_2) are calculated to be 0.26 dB μm^{-1} and 0.27 dB μm^{-1} respectively, thus revealing that the optical waveguide property is isotropic in BTCs.

Our observations of 2D optical waveguide properties based on BTCs are very different from previous work.[21,42] Heng and co-workers[42] demonstrate the 2D optical waveguide of hexaphenylsilole (HPS) crystals with an intersection angle of 90° between the two propagation directions, while Zhao and co-workers[21] declare an asymmetric behavior on the rhombic crystal of 2-acetyl-6-methylaminonaphthalene (AMN). Both of them attribute the unique optical waveguide properties to the molecular packing structures of the crystals. However, it does not seem to be the case in our BTC system because photons propagated in different directions with distinct molecular stacking structures show similar loss coefficient. Here we propose that the optical waveguide property of the organic crystal is not related to the molecular packing structure, but somehow it is shape- and dimension-dependent. When an organic crystal served as an optical waveguide, the PL propagation directions were determined by its morphology. And total reflection happens along these distinct propagation directions with almost equal absorption and scattering of photons because of the identical crystal circumstances, thus leading to similar optical loss. In this regard, isotropic PL propagation in this 2D BTC is expected.

In conclusion, a new light-emitting cocrystal of a CT complex (1:1), with a 2D parallelogram-like shape, was obtained by molecular self-assembly. The CT, π–π, -N···HC- interactions are the driving forces for assembly and are responsible for the resulting 2D morphology. The CT nature of the BTCs was confirmed by experimental and theoretical evidence, and the results display that both the ground and excited state are CT states. The lowest CT_0 to CT_1 electronic transition arises from the HOMO to LUMO excitation, while the generated CT_1 excitons recombine to give a strong violet-blue luminescence with PLQY of 19%. Moreover, the excited PL can actively propagate in the individual 2D cocrystal without anisotropy, thus indicating that the optical waveguide property of organic crystals has nothing to do with their molecular packing structures. This unique CT cocrystal shows promising applications in photonic resistors and planar-light propagation directional modulators, which can be integrated into functional photonic circuits for the next-generation optoelectronic communications. More importantly, our research shows an excellent example of how to understand the CT interactions in organic D–A systems and provides valuable insight into rational design and supramolecular synthesis of organic cocrystals with desired morphologies and functions.

Keywords: charge transfer · crystal engineering · density functional calculations · donor–acceptor systems · self-assembly

How to cite: *Angew. Chem. Int. Ed.* **2015**, *54*, 6785–6789
Angew. Chem. **2015**, *127*, 6889–6893

[1] A. K. Blackburn, A. C. H. Sue, A. K. Shveyd, D. Cao, A. Tayi, A. Narayanan, B. S. Rolczynski, J. M. Szarko, O. A. Bozdemir, R. Wakabayashi, J. A. Lehrman, B. Kahr, L. X. Chen, M. S. Nassar, S. I. Stupp, J. F. Stoddart, *J. Am. Chem. Soc.* **2014**, *136*, 17224–17235.

[2] S. K. Park, S. Varghese, J. H. Kim, S.-J. Yoon, O. K. Kwon, B.-K. An, J. Gierschner, S. Y. Park, *J. Am. Chem. Soc.* **2013**, *135*, 4757–4764.

[3] H. L. Nguyen, P. N. Horton, M. B. Hursthouse, A. C. Legon, D. W. Bruce, *J. Am. Chem. Soc.* **2004**, *126*, 16–17.

© 2015 Wiley-VCH Verlag GmbH & Co. KGaA, Weinheim

[4] M. Morimoto, M. Irie, *J. Am. Chem. Soc.* **2010**, *132*, 14172 – 14178.
[5] O. Bolton, K. Lee, H.-J. Kim, K. Y. Lin, J. Kim, *Nat. Chem.* **2011**, *3*, 205 – 210.
[6] F. Pan, M. S. Wong, V. Gramlich, C. Bosshard, P. Günter, *J. Am. Chem. Soc.* **1996**, *118*, 6315 – 6316.
[7] G. R. Desiraju, *CrystEngComm* **2003**, *5*, 466 – 467.
[8] J. D. Dunitz, *CrystEngComm* **2003**, *5*, 506 – 506.
[9] C. B. Aakeröy, D. J. Salmon, *CrystEngComm* **2005**, *7*, 439 – 448.
[10] S. Horiuchi, F. Ishii, R. Kumai, Y. Okimoto, H. Tachibana, N. Nagaosa, Y. Tokura, *Nat. Mater.* **2005**, *4*, 163 – 166.
[11] W. Yu, X.-Y. Wang, J. Li, Z.-T. Li, Y.-K. Yan, W. Wang, J. Pei, *Chem. Commun.* **2013**, *49*, 54 – 56.
[12] Y. L. Lei, L. S. Liao, S. T. Lee, *J. Am. Chem. Soc.* **2013**, *135*, 3744 – 3747.
[13] J. Ferraris, D. O. Cowan, V. Walatka, J. H. Perlstein, *J. Am. Chem. Soc.* **1973**, *95*, 948 – 949.
[14] Y. Qin, J. Zhang, X. Zheng, H. Geng, G. Zhao, W. Xu, W. Hu, Z. Shuai, D. Zhu, *Adv. Mater.* **2014**, *26*, 4093 – 4099.
[15] Y. L. Lei, Y. Jin, D. Y. Zhou, W. Gu, X. B. Shi, L. S. Liao, S.-T. Lee, *Adv. Mater.* **2012**, *24*, 5345 – 5351.
[16] J. D. Wuest, *Nat. Chem.* **2012**, *4*, 74 – 75.
[17] D. Yan, H. Yang, Q. Meng, H. Lin, M. Wei, *Adv. Funct. Mater.* **2014**, *24*, 587 – 594.
[18] D. Yan, A. Delori, G. O. Lloyd, T. FriŠčić, G. M. Day, W. Jones, J. Lu, M. Wei, D. G. Evans, X. Duan, *Angew. Chem. Int. Ed.* **2011**, *50*, 12483 – 12486; *Angew. Chem.* **2011**, *123*, 12691 – 12694.
[19] H. Jiang, K. K. Zhang, J. Ye, F. Wei, P. Hu, J. Guo, C. Liang, X. Chen, Y. Zhao, L. E. McNeil, W. Hu, C. Kloc, *Small* **2013**, *9*, 990 – 995.
[20] X. Wang, Q. Liao, Q. Kong, Y. Zhang, Z. Xu, X. Lu, H. Fu, *Angew. Chem. Int. Ed.* **2014**, *53*, 5863 – 5867; *Angew. Chem.* **2014**, *126*, 5973 – 5977.
[21] W. Yao, Y. Yan, L. Xue, C. Zhang, G. Li, Q. Zheng, Y. S. Zhao, H. Jiang, J. Yao, *Angew. Chem. Int. Ed.* **2013**, *52*, 8713 – 8717; *Angew. Chem.* **2013**, *125*, 8875 – 8879.
[22] M. Pope, *Electronic Processes in Organic Crystals and Polymers*, 2nd ed., Oxford University Press, Oxford, **1999**.
[23] J. B. Torrance, *Acc. Chem. Res.* **1979**, *12*, 79 – 86.
[24] G. D′Avino, M. J. Verstraete, *Phys. Rev. Lett.* **2014**, *113*, 237602.
[25] A. D. Bandrauk, K. D. Truong, C. Carlone, *Can. J. Chem.* **1982**, *60*, 588 – 595.
[26] A. D. Bandrauk, K. D. Truong, V. R. Salares, H. J. Bernstein, *J. Raman Spectrosc.* **1979**, *8*, 5 – 10.
[27] J. Zhang, J. H. Tan, Z. Y. Ma, W. Xu, G. Y. Zhao, H. Geng, C. A. Di, W. P. Hu, Z. G. Shuai, K. Singh, D. B. Zhu, *J. Am. Chem. Soc.* **2013**, *135*, 558 – 561.
[28] J. Zhang, H. Geng, T. S. Virk, Y. Zhao, J. H. Tan, C. A. Di, W. Xu, K. Singh, W. P. Hu, Z. G. Shuai, Y. Q. Liu, D. B. Zhu, *Adv. Mater.* **2012**, *24*, 2603 – 2607.
[29] G. Agostini, C. Corvaja, G. Giacometti, L. Pasimeni, D. A. Clemente, *J. Phys. Chem.* **1988**, *92*, 997 – 1003.
[30] S. Iwata, J. Tanaka, S. Nagakura, *J. Am. Chem. Soc.* **1967**, *89*, 2813 – 2819.
[31] S. M. Hubig, J. K. Kochi, *J. Phys. Chem.* **1995**, *99*, 17578 – 17585.
[32] M. Samoc, D. F. Williams, *J. Chem. Phys.* **1983**, *78*, 1924 – 1930.
[33] J. y. Tsutsumi, H. Matsui, T. Yamada, R. Kumai, T. Hasegawa, *J. Phys. Chem. C* **2012**, *116*, 23957 – 23964.
[34] R. J. Dillon, C. J. Bardeen, *J. Phys. Chem. A* **2011**, *115*, 1627 – 1633.
[35] C. L. Braun, *J. Chem. Phys.* **1984**, *80*, 4157 – 4161.
[36] F. Masetti, G. Bartocci, U. Mazzucato, E. Fischer, *J. Chem. Soc. Perkin Trans. 2* **1983**, 797 – 802.
[37] S. Iwata, J. Tanaka, S. Nagakura, *J. Am. Chem. Soc.* **1966**, *88*, 894 – 902.
[38] Y. Li, W. Wang, W. R. Leow, B. Zhu, F. Meng, L. Zheng, J. Zhu, X. Chen, *Small* **2014**, *10*, 2776 – 2781.
[39] D. Zhang, L. Luo, Q. Liao, H. Wang, H. Fu, J. Yao, *J. Phys. Chem. C* **2011**, *115*, 2360 – 2365.
[40] Z. Z. Xu, Q. Liao, Q. Shi, H. L. Zhang, J. N. Yao, H. B. Fu, *Adv. Mater.* **2012**, *24*, OP216 – OP220.
[41] J. Zhang, B. Xu, J. Chen, S. Ma, Y. Dong, L. Wang, B. Li, L. Ye, W. Tian, *Adv. Mater.* **2014**, *26*, 739 – 745.
[42] L. Heng, X. Wang, D. Tian, J. Zhai, B. Tang, L. Jiang, *Adv. Mater.* **2010**, *22*, 4716 – 4720.

Received: February 12, 2015
Revised: March 6, 2015
Published online: April 20, 2015

 © 2015 Wiley-VCH Verlag GmbH & Co. KGaA, Weinheim